RSC Advances

ROYAL SOCIETY OF CHEMISTRY

www.rsc.org/advances

Cite this: DOI: 10.1039/c0xx00000x

www.rsc.org/xxxxxx

ARTICLE TYPE

Luminescent and Magnetic Properties of the Afterglow Phosphors $GdSr_2AlO_5:RE^{3+}$ (RE^{3+} = Eu^{3+}, Sm^{3+}, Pr^{3+} and Dy^{3+})

Gen Li, Yuhua Wang,* Wei Zeng, Wenbo Chen, Shaochun Han and Haijie Guo

Received (in XXX, XXX) Xth XXXXXXXXX 20XX, Accepted Xth XXXXXXXXX 20XX

DOI: 10.1039/b000000x

Novel afterglow phosphors based on $GdSr_2AlO_5$ host were prepared by a solid-state reaction under a reductive atmosphere. The PL, afterglow, TL and magnetism properties of $GdSr_2AlO_5:RE^{3+}$ (RE^{3+} = Eu^{3+}, Sm^{3+}, Pr^{3+} and Dy^{3+}) were discussed in detail for the first time in this paper. By doping appropriate rare earth ions into the $GdSr_2AlO_5$ host, all phosphors showed a satisfactory long-wavelength afterglow phenomenon and excellent paramagnetism characteristics simultaneously. The mass magnetic susceptibility value was determined to be approximately 4.4052×10^{-5} emu/(g • Oe).

1. Introduction

Long lasting phosphorescence (LLP) materials relate to a particular optical phenomenon in which the excitation energy can be stored and then slowly released by a photonic emission for several minutes or hours after the stoppage of the excitation.[1,2] Due to the unique luminescent characteristics and many advantages such as energy saving and environmental protection, LLP materials have attracted hectic researches in recent years.

At present, with the rapid development of LLP materials, they have been widely used in many areas. Initially, LLP materials are applied to security signs, emergency route signs, traffic signage and night displays. These materials are also utilized in optical storage media, radiation detection and structural damage sensors.[3,4,5] Up to now, more and more fields, especially in the biomedical applications, can use LLP materials to solve relevant questions such as in vivo optical imaging.[6,7,8] The afterglow in these materials could last several hours after being optically excited in vitro. And their in vivo distribution could be detected in real time after the injection without the need for any external illumination source. Thus, the signal-to-noise ratio could be significantly improved due to the avoidance of the autofluorescence in tissue organic components, originating from in situ excitation.[9] But there are still some shortcomings such as low resolution. Fortunately, another important non-invasive diagnostic imaging, namely magnetic resonance imaging, provides excellent opaque tissue contrast and spatial resolution, which just could make up for the main shortcoming.[10,11] Recently, Shi et al. reported a new core/shell structure Gd_2O_3@$mSiO_2$@$CaTiO_3$:Pr that integrated optical imaging with magnetic resonance imaging, which provided an approach to bridge the gap in resolution, sensitivity and depth of imaging.[12] In this approach, $CaTiO_3$:Pr provided the afterglow and Gd_2O_3 provided the magnetism. Nevertheless, the combination of several materials maybe suffer from complexities associated with the synthesis of the core/shell structure. Therefore, to develop a LLP material which possesses magnetism, should be significant and meaningful for the potential application in biomedical imaging.

Additionally, in order to avoid being absorbed by tissue organic components, the probe's emission of LLP materials should be tuned in the tissue transparency window, namely, the wavelength range from 650 nm to the infrared.[13] At present, there is only some ions such as Cr^{3+} due to the excellent infrared emission, investigated and applied in the field of biomedical imaging.[8,14] Other ions are reported rarely. But in fact, both Eu^{3+} and Sm^{3+} could have a long-wavelength emission above 650 nm. Although their emissions below are strong as well, they will be absorbed and have no affect on the probe. Thus, these rare earth (RE) ions could be selected as the emission centers for the phosphorescence. Recently, the $GdSr_2AlO_5:Ce^{3+}$ phosphor on a nanoscale-particle size prepared successfully by a sol-gel method was reported by Jin Young Park et al..[15] In addition, the structural and optical properties of the Ce^{3+} doped solid solutions between two isotypic host compounds: $GdSr_2AlO_5$ and Sr_3AlO_4F were also investigated.[16] Upon going through the literature, it is clear that, with the exception of the Ce^{3+} doped $GdSr_2AlO_5$ phosphor, any other RE ion doped $GdSr_2AlO_5$ phosphors have not been studied so far and there is no report on their afterglow property. In this article, various RE ion doped $GdSr_2AlO_5$ phosphors were obtained successfully by a solid state reaction under a reductive atmosphere and identified by XRD refinement. The photoluminescence, afterglow, thermoluminescence and magnetism properties of $GdSr_2AlO_5:RE^{3+}$ (RE^{3+} = Eu^{3+}, Sm^{3+}, Pr^{3+} and Dy^{3+}) phosphors were investigated in detail for the first time.

2. Experimental

2.1. Synthesis

The $GdSr_2AlO_5:RE^{3+}$ (RE^{3+} = Eu^{3+}, Sm^{3+}, Pr^{3+} and Dy^{3+})

phosphors were synthesized by conventional high temperature solid state reaction method. The raw materials Gd_2O_3 (99.9%), $SrCO_3$ (99.9%), Al_2O_3 (99.9%) and RE oxides (Eu_2O_3, Sm_2O_3, Pr_6O_{11} and Dy_2O_3 purity) were stoichiometrically weighted out. After the ingredients were mixed thoroughly, the mixtures were placed into an alumina crucible and sintered at 1500℃ for 4 h under a reductive atmosphere (5% H_2 + 95% N_2) in an electric tube furnace. Finally, after calcination, the samples were cooled to room temperature in the furnace and ground again into powder for subsequent use.

2.2. Characterization

The phases of samples were identified by X-ray powder diffraction (XRD, Rigaku D/MaX-2400) with Ni-filtered Cu Kα radiation at a scanning step of 0.02° in the 2θ range from 10° to 80°. The morphology of the sample and the energy dispersive X-ray spectroscopy (EDS) spectrum were detected by field emission scanning electron microscopy (FESEM, Hitachi, S-4800). Photoluminescence emission (PL) and excitation (PLE) spectra were carried out by a FLS-920T spectrometer. The scanning step was 1 nm. Afterglow decay curve measurements were measured with a PR305 long afterglow instrument after the samples were irradiated with standard artificial daylight for 10 min. Thermoluminescence (TL) curves were measured with a FJ-427A TL meter (Beijing Nuclear Instrument Factory) with a heating rate of 1 K s^{-1}. The sample weight was kept constant (20 mg). Before the measurements, the samples were irradiated with ultraviolet light (254 nm) for 10 min. Magnetism properties were measured using a vibrating sample magnetometer (VSM, Lake-Shore 7400 Series). All the measurements were carried out at room temperature except for TL curves and magnetization curves. The results are repeatable.

3. Results and discussion

3.1. Phase analysis

Fig. 1a shows Rietveld structural refinement of the XRD pattern of $GdSr_2AlO_5$ host, obtained using MS program. Red solid line, black crosses and blue solid line are the calculated pattern, experimental pattern and background, respectively. Pink short vertical lines show the positions of Bragg reflections of the calculated pattern. The difference between experimental and calculated pattern is plotted by dark cyan line at the bottom. For the structure refinement, initial structural model is constructed with the crystallographic data of $EuSr_2AlO_5$[17], which approximates actual crystal structure of $GdSr_2AlO_5$. The final refinement residual factors are R_{wp} = 6.25% and R_p = 4.67%. The refinement results confirm the single-phase nature of the compound in the tetragonal space group I4/mcm (No. 140) with cell parameters a = b = 6.6435(0) Å and c = 10.7901(1) Å. Compared with $EuSr_2AlO_5$ (a = b = 6.7421 Å and c = 10.9700 Å)[17], $GdSr_2AlO_5$ has a contracted tetragonal cell, in agreement with the ionic radius of 8-coordinate Gd^{3+} (1.053 Å) being smaller than that of Eu^{3+} (1.066 Å)[18]. Fig. 1b shows the EDS spectrum analysis of the $GdSr_2AlO_5$ sample. It confirms the presence of gadolinium (Gd), strontium (Sr), aluminium (Al), oxygen (O), and carbon (C) in the $GdSr_2AlO_5$ sample. Except for C, which is deduced from the use of conductive adhesive tape for supporting the sample, no other impurity peaks can be detected. The SEM image of $GdSr_2AlO_5$ host is shown in the inset of Fig. 1b. It is clearly seen that the grains have irregular shape of blocky particles with a size of about 2-7 μm.

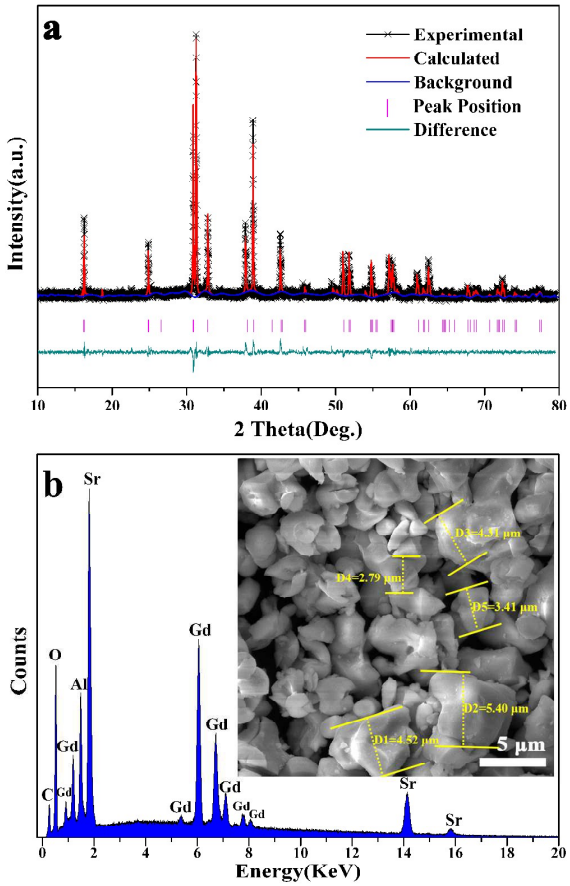

Fig. 1 (a) XRD refinement results of $GdSr_2AlO_5$ host. (b) the EDS spectrum of $GdSr_2AlO_5$ host. The inset shows SEM image of $GdSr_2AlO_5$ host.

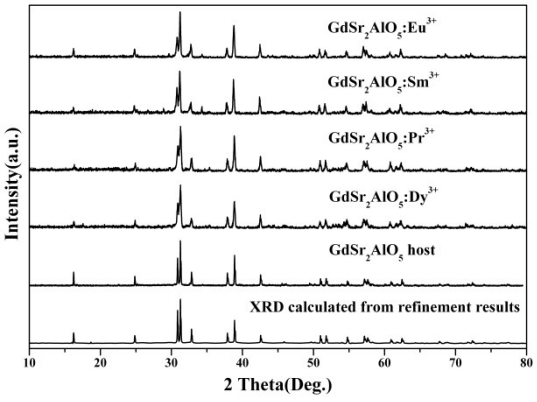

Fig. 2 XRD patterns of $GdSr_2AlO_5$ host, $GdSr_2AlO_5$:RE^{3+} (RE^{3+} = Eu^{3+}, Sm^{3+}, Pr^{3+} and Dy^{3+}) and the calculated XRD pattern from the refinement results.

Fig. 2 shows the XRD patterns of various RE ion doped $GdSr_2AlO_5$ phosphors as well as the experimental and calculated XRD patterns of $GdSr_2AlO_5$ host according to the refinement results. In the present study, the RE ion contents in all phosphors are fixed at 1% of Gd. It is obvious that the XRD profiles are well fitted with the calculated XRD pattern and diffraction peaks of

Cite this: DOI: 10.1039/c0xx00000x

www.rsc.org/xxxxxx

ARTICLE TYPE

these phosphors can be exactly assigned to $GdSr_2AlO_5$ host. No detectable impurity phase is observed in all obtained phosphors, indicating the RE ions (RE^{3+} = Eu^{3+}, Sm^{3+}, Pr^{3+} and Dy^{3+}) have been successfully incorporated in the host lattice without changing the crystal structure largely.

3.2. Photoluminescence analysis

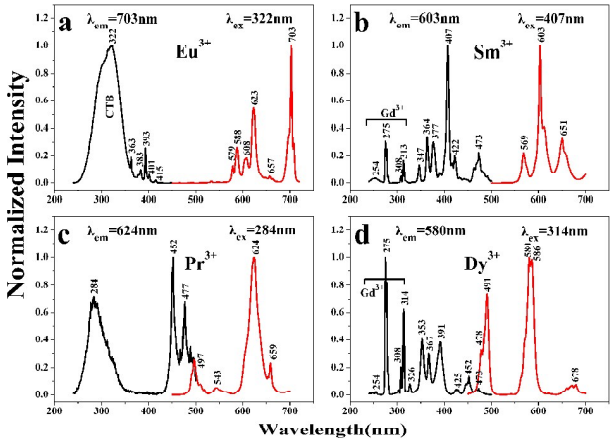

Fig. 3 (a-d) PLE (black) and PL (red) spectra of $GdSr_2AlO_5:RE^{3+}$ (RE^{3+} = Eu^{3+}, Sm^{3+}, Pr^{3+} and Dy^{3+}).

The room-temperature PLE and PL spectra of $GdSr_2AlO_5:RE^{3+}$ (RE^{3+} = Eu^{3+}, Sm^{3+}, Pr^{3+} and Dy^{3+}) are presented in Fig. 3. These phosphors show characteristic excitation and emission peaks, attributed to different electronic transitions of trivalent RE ions.[19-24]

When monitored at 703 nm, the PLE spectrum of $GdSr_2AlO_5:Eu^{3+}$ in Fig. 3a shows a broad band near 322 nm, ascribed to Eu^{3+}-O^{2-} charge transfer band (CTB), which corresponds to an electron transferred from oxygen 2p orbital to the empty 4f orbital of Eu^{3+}. The five sharp excitation peaks can be attributed to the Eu^{3+} intra-4f transitions, which correspond to the $^5D_0$-$^7F_1$ (363 nm), $^5D_0$-$^7F_2$ (383 nm), $^5D_0$-$^7F_3$ (393 and 401 nm) and $^5D_0$-$^7F_4$ (415 nm), respectively. Upon 322 nm excitation, the PL spectrum shows some sharp emission peaks of Eu^{3+}, ascribed to the $^5D_0$-$^7F_1$ (579 and 588 nm), $^5D_0$-$^7F_2$ (608 and 523 nm), $^5D_0$-$^7F_3$ (657 nm) and $^5D_0$-$^7F_4$ (703 nm), respectively. The electric-dipole transition ($^5D_0$-$^7F_2$) is stronger than the magnetic-dipole transition ($^5D_0$-$^7F_1$), indicating that Eu^{3+} ions occupy a low-symmetry site.[25,26]

What's more, in $GdSr_2AlO_5:Eu^{3+}$ the $^5D_0$-$^7F_4$ transition at 703 nm is strongest, which is greatly appropriate for the application in biomedical imaging.[13] Generally, the dominant transition from $^5D_0$-$^7F_4$ are not so often found in PL spectrum of Eu^{3+} ions. It is suggested that a highly polarizable chemical environment corresponds to a coordination polyhedron of Eu^{3+} ions in $GdSr_2AlO_5$. The abnormal high intensities of the $^5D_0$-$^7F_4$ transition are likely due to the distortion of the Eu^{3+} local-symmetry group.[27,28]

Fig. 3b shows the PLE and PL spectra of $GdSr_2AlO_5:Sm^{3+}$. By monitoring the room temperature emission at 603 nm due to the $^4G_{5/2}$-$^6H_{7/2}$ transition, a group of sharp lines at 250-500 nm are detected in the PLE spectrum. The first four sharp excitation peaks can be attributed to the Gd^{3+} typical transitions of $^8S_{7/2}$-^6D_J (254 nm), $^8S_{7/2}$-^6I_J (275 nm) and $^8S_{7/2}$-^6P_J (308 and 311 nm), which also exist in the PLE spectrum of $GdSr_2AlO_5:Dy^{3+}$ in Fig. 3d. The other peaks are ascribed to the Sm^{3+} f-f forbidden transitions of $^6H_{5/2}$-(^4K, $^4L)_{17/2}$ (347 nm), $^6H_{5/2}$-(^4D, $^6P)_{15/2}$ (364 nm), $^6H_{5/2}$-$^4L_{17/2}$ (377 nm), $^6H_{5/2}$-$^4K_{11/2}$ (the strongest sharp line 407 nm), $^6H_{5/2}$-(^4P, $^6P)_{5/2}$ (422 nm) and $^6H_{5/2}$-$^4I_{13/2}$, ($^4I_{9/2}$) (473 nm), respectively. The PL spectrum of $GdSr_2AlO_5:Sm^{3+}$ under excitation of 407 nm is also shown in Fig. 3b. There are three prominent groups of emission lines approximately in the range of 550 to 700 nm, which can be attributed to the Sm^{3+} intra-4f orbital transition of $^4G_{5/2}$-$^6H_{5/2}$ (569 nm), $^4G_{5/2}$-$^6H_{7/2}$ (603 nm) and $^4G_{5/2}$-$^6H_{9/2}$ (651 nm), respectively. Among them, the $^4G_{5/2}$-$^6H_{7/2}$ (603 nm) transition has the strongest emission intensity.

When 624 nm emission of Pr^{3+} is monitored, PLE spectrum is recorded in Fig. 3c and composed of two main parts. One is a prominent band locating at 284 nm, which can be ascribed to the 4f-5d transition of Pr^{3+}. Another part is from 400 to 500 nm with several sharp peaks, which are attributed to 4f-4f transition Pr^{3+} ions. Among them the two strong relatively excitation peaks at 451 nm and 475 nm are corresponding to transitions from $^3H_4$ to $^3P_2$ and $^3P_1$. The PL spectrum shows that four peaks are located at 497 nm, 543 nm, 624 nm and 659 nm, corresponding to the Pr^{3+} transitions of $^3P_0$-$^3H_4$, $^3P_0$-$^3H_5$, $^1D_2$-$^3H_4$ and $^3P_0$-$^3F_2$, respectively. As is well known, the 4f-4f transitions are more probable when the Pr^{3+} ions are located in low-symmetry sites inside the crystalline host lattice.[29] Among all emission peaks, the peak at 624 nm ($^1D_2$-$^3H_4$) originated by the forbidden 4f-4f intra-shell transition possesses the maximum intensity, which obviously indicates that the Pr^{3+} ions occupy a low-symmetry site.

Fig. 3d shows the PLE and PL spectra of $GdSr_2AlO_5:Dy^{3+}$. The PLE spectrum is monitored at 580 nm in the range of 250-500 nm. In addition to the four above-mentioned sharp peaks corresponding to the Gd^{3+} transitions, the others come from the ground state of $^6H_{15/2}$ to the excited states of $4f^9$ electronic configurations of Dy^{3+}, which are located at 326 nm ($^6H_{15/2}$-$^4M_{17/2}$), 353 nm ($^6H_{15/2}$-$^6P_{7/2}$), 367 nm ($^6H_{15/2}$-$^4I_{11/2}$), 391 nm ($^6H_{15/2}$-$^4I_{13/2}$), 425 nm ($^6H_{15/2}$-$^4G_{11/2}$), 452 nm ($^6H_{15/2}$-$^4I_{15/2}$) and 473 nm ($^6H_{15/2}$-$^4F_{9/2}$), respectively. The PL spectrum exhibits three peaks corresponding to $^4F_{9/2}$-$^6H_{15/2}$ (478 and 491 nm), $^4F_{9/2}$-$^6H_{13/2}$ (580 and 586 nm) and $^4F_{9/2}$-$^6H_{11/2}$ (678 nm) of Dy^{3+}, respectively. It is well known that the $^4F_{9/2}$-$^6H_{15/2}$ magnetic-dipole transition is prominent when Dy^{3+} is located at a high-symmetry site, while the $^4F_{9/2}$-$^6H_{13/2}$ electric-dipole transition is stronger when Dy^{3+} is located at a low-symmetry site. In our case, the emission at 580 nm ($^4F_{9/2}$-$^6H_{13/2}$) is stronger than the emission at 491 nm ($^4F_{9/2}$-$^6H_{15/2}$), which illustrates that Dy^{3+} occupies a low-symmetry site.[30,31] Additionally, the energy-level splitting of $^4F_{9/2}$-$^6H_{15/2}$ and $^4F_{9/2}$-$^6H_{13/2}$ caused by the crystal field interaction

also has great relation to the low-symmetry site for the substitution[22,25], which matches the previous analysis.

The conclusions about the occupancy for RE ions are consistent with each other and uniformly show that the incorporated RE ions occupy a low-symmetry site in the $GdSr_2AlO_5$ host. It's worth mentioning that, in this work all $GdSr_2AlO_5:RE^{3+}$ phosphors obtain a long-wavelength emission, which could make up for the shortage of long-wavelength emission LLP materials. Thus, their afterglow properties are investigated respectively.

3.3. Afterglow characteristic

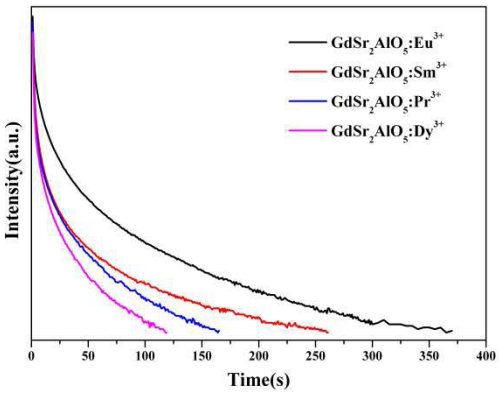

Fig. 4 The afterglow decay curves of $GdSr_2AlO_5:RE^{3+}$ (RE^{3+} = Eu^{3+}, Sm^{3+}, Pr^{3+} and Dy^{3+}).

Fig. 4 depicts the afterglow decay curves of $GdSr_2AlO_5:RE^{3+}$ (RE^{3+} = Eu^{3+}, Sm^{3+}, Pr^{3+} and Dy^{3+}). Doping different RE ions, the four phosphors exhibit the afterglow for several minutes, and $GdSr_2AlO_5:Eu^{3+}$ possesses the best afterglow performance among them. The prone afterglow phenomenon implies that $GdSr_2AlO_5$ could be an excellent host matrix for the design of LLP materials.

All these phosphors are evaluated by measuring their afterglow as a function of time in photometric units. The extinction time is defined as the time until the luminance has decayed to 0.32 mcd/m^2, which is roughly 100 times the eye sensitivity in dark-adapted condition.[32] However, the eye sensitivity curve shifts from photopic vision to scotopic vision upon decreasing light intensity, with a corresponding decrease in red-sensitivity. Thus, the performance of these long-wavelength LLP materials cannot be described accurately with the photometry.[33] Especially, the infrared such as the emission at 703 nm in the $GdSr_2AlO_5:Eu^{3+}$ phosphor, is more difficult to be detected in this way. So it is possible that their afterglow time should be much more than the obtained above.

3.4. Thermoluminescence characteristics

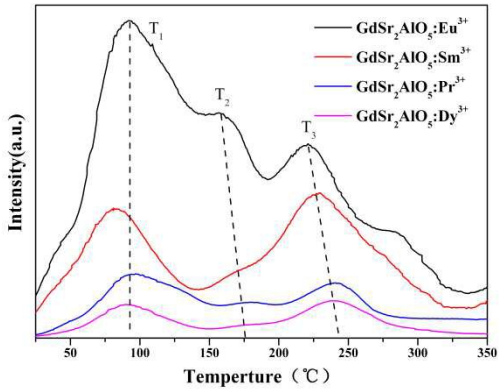

Fig. 5 TL curves of $GdSr_2AlO_5:RE^{3+}$ (RE^{3+} = Eu^{3+}, Sm^{3+}, Pr^{3+} and Dy^{3+}).

It is well known that energy traps play an essential role for photoenergy storage in LLP materials, which have great effect on the afterglow performance.[34] In general, TL technique is a very useful tool to obtain the information with regard to the energy trap depth and density.[35] Fig. 5 represents the TL curves of $GdSr_2AlO_5:RE^{3+}$ (RE^{3+} = Eu^{3+}, Sm^{3+}, Pr^{3+} and Dy^{3+}). All curves show three TL peaks at the same positions approximately, corresponding to 90 ℃ (T_1), 170 ℃ (T_2) and 230 ℃ (T_3), respectively. It is well known that the TL peak at somewhere between 50 and 120℃ is suitable for LLP materials to free the trapped carriers slowly by thermal energy at room temperature.[36,37] So neither T_2 nor T_3 is appropriate for creating afterglow phenomenon. T_1 traps at 90℃ are exactly the traps which lead to the afterglow phenomenon in all different RE ion single-doped phosphors.

The thermally stimulated persistent luminescence in these phosphors is very sensitive to ambient temperatures. To obtain a good afterglow performance, the appropriate trap depths should be related to the working temperatures. The temperature is approximately 38℃ in some living biological tissues. It is higher than the as-defined room temperature at approximately 20℃.[38] Generally, in the TL curve the traps at near 70℃, corresponding to the room temperature at 20℃, would be the most appropriate for the afterglow performance.[39,40] Therefore, these LLP materials with the traps at relatively high temperature 90℃ could be suitable when used in biomedical imaging at 38℃.

Additionally, in this investigation the incorporation of different RE ion basically doesn't change the energy trap depth, which indicates that these traps could be related to the defects from intrinsic nature of $GdSr_2AlO_5$ host. Generally, in high temperature and reductive atmosphere, oxygen atoms may be missed easily and then become oxygen vacancies.[41,42] So it is considered that the traps are related to oxygen vacancies, which were also found in the previously reported $Sr_2SnO_4:Sm^{3+}$ [43] and $Gd_{9.33}(SiO_4)_6O_2:Sm^{3+}$ [25]. These oxygen vacancies can act as electron traps in LLP materials, which should play major roles in the initial intensity and persistent time.[43] In the TL curve, the intensity corresponds to the quantity of traps. Compare Fig. 4 with Fig. 5, it could be found that among the four different phosphors, the one with more oxygen vacancies possesses longer afterglow time, which is in coincidence with previous reports[25,43]. Nevertheless, these trap intensities are so weak that they directly result in the short afterglow, and it is hard to identify the traps' nature from the present data. Thus in the future research, more

Cite this: DOI: 10.1039/c0xx00000x

www.rsc.org/xxxxxx

ARTICLE TYPE

methods such as appropriate doping and co-doping should be used to improve the afterglow properties of $GdSr_2AlO_5$ phosphors, and further investigations on the identification of traps are necessary to clarify the afterglow mechanism.

3.5. Magnetism characteristics

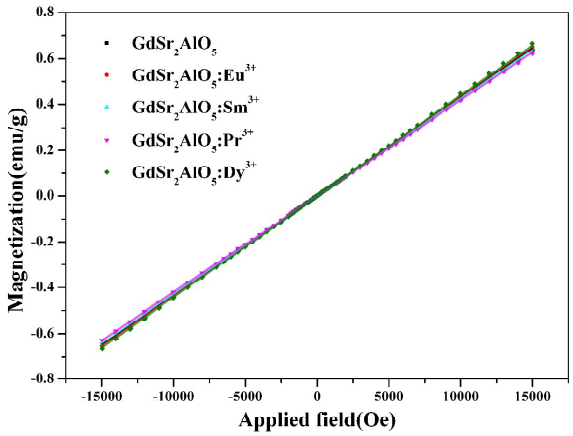

Fig. 6 Magnetization as a function of applied field for $GdSr_2AlO_5$ and $GdSr_2AlO_5:RE^{3+}$ (RE^{3+} = Eu^{3+}, Sm^{3+}, Pr^{3+} and Dy^{3+}) at room temperature.

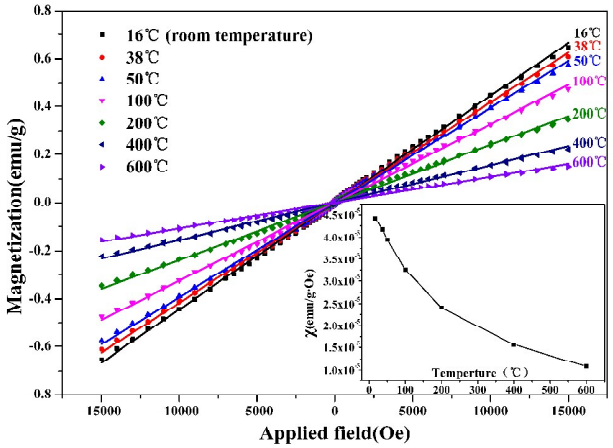

Fig. 7 Magnetization as a function of applied field for $GdSr_2AlO_5$ host at different temperature. The inset shows the dependence of magnetic susceptibility on temperature.

Besides PL, afterglow and TL, the magnetism properties of $GdSr_2AlO_5$ and $GdSr_2AlO_5:RE^{3+}$ (RE^{3+} = Eu^{3+}, Sm^{3+}, Pr^{3+} and Dy^{3+}) are also investigated. To our knowledge, this is the first report on the paramagnetism properties of $GdSr_2AlO_5$ and $GdSr_2AlO_5:RE^{3+}$. Measurement of the magnetization as a function of applied field at room temperature is shown in Fig. 6. As the strength of the applied magnetic field increases, the ideal linear correlations between the magnetization and the applied magnetic field in the $GdSr_2AlO_5$ and $GdSr_2AlO_5:RE^{3+}$ are obtained, indicating that they possess paramagnetism. The paramagnetism properties could come from Gd^{3+}, rather than the incorporated RE ions. This is due to the fact that Gd^{3+} possesses seven unpaired inner 4f electrons.[44] As can been seen from Fig. 6, the incorporated RE ions have little influence on the paramagnetism property, so the four magnetization curves of $GdSr_2AlO_5:RE^{3+}$ almost overlap with that of $GdSr_2AlO_5$ and all mass magnetic susceptibility value is determined to be approximately 4.4052×10^{-5} emu/(g·Oe). The value approach those of $NaGd(WO_4)_2:Tb^{3+}$ (4.46×10^{-5} emu/(g·Oe))[45] and $BaGdF_5:Yb^{3+}/Er^{3+}$ (4.72×10^{-5} emu/(g·Oe))[46]. The magnetization at 10 kOe is around 0.44052 emu/g.

Fig. 7 shows the magnetization as a function of applied field for $GdSr_2AlO_5$ at different temperature from 16 to 600℃. The mass magnetic susceptibility value is determined and shown in the inset of Fig. 7, respectively. It could be found that the magnetic susceptibility of $GdSr_2AlO_5$ host decreases gradually with the ascension of temperature, which conforms to the Curie's law.[47] The mass magnetic susceptibility value is 4.1742×10^{-5} emu/(g·Oe) at 38℃.

4. Conclusions

In summary, novel afterglow phosphors based on $GdSr_2AlO_5$ host are successfully synthesized by a solid state reaction. The PL, afterglow, TL and magnetism properties of $GdSr_2AlO_5:RE^{3+}$ (RE^{3+} = Eu^{3+}, Sm^{3+}, Pr^{3+} and Dy^{3+}) are discussed in detail for the first time. All obtained phosphors show a long-wavelength emission at approximately 600 nm, and exhibit the afterglow for several minutes. In addition, they show excellent paramagnetism characteristics simultaneously with the mass magnetic susceptibility value at 4.4052×10^{-5} emu/(g·Oe). So the red-emitting, paramagnetic and LLP $GdSr_2AlO_5:RE^{3+}$ should be promising candidates for multifunctional applications.

Acknowledgments

This work is supported by Specialized Research Fund for the Doctoral Program of Higher Education (Grant No.20120211130003) and the National Natural Science Funds of China (Grant No. 51372105).

Notes and references

*Department of Materials Science, School of Physical Science and Technology, Lanzhou University, Lanzhou, 730000, PR China and Key Laboratory for Special Function Materials and Structural Design of the Ministry of Education, Lanzhou University, Lanzhou 730000, China. *Corresponding author: Yuhua Wang*

Email address: wyh@lzu.edu.cn; tel.: +86 931 8912772; fax: +86 931 8913554.

1. Z. Pan, Y. Y. Lu and F. Liu, Nat. Mater., 2012, 11, 58-63.

2. X. Yu, X. Xu, H. Yu, T. Jiang, P. Yang, Q. Jiao and J. Qiu, Mater. Res. Bull., 2012, 47, 2696-2699.

3. H.A. Hoppe, H. Lutz, P. Morys, W. Schnick and A. Seilmeier, J. Phys. Chem. Solids, 2000, 61, 2001-2006.

4. M. Kowatari, D. Koyama, Y. Satoh, K. Iinuma and S. Uchida, Nucl. Instrum. Methods Phys. Res., Sect. A, 2002, 480, 431-439.

5. C. N. Xu, T. Watanabe, M. Akiyama and X. G. Zheng, Appl. Phys. Lett., 1999, 74, 2414-2416.
6. S. Lian, Y. Qi, C. Rong, L. Yu, A. Zhu, D. Yin and S. Liu, J. Phys. Chem. C, 2010, 114, 7196-7204.
7. Q. L. de Chermont, C. Chaneac, J. Seguin, F. Pelle, S. Maitrejean, J. P. Jolivet, D. Gourier, M. Bessodes and D. Scherman, Proc. Natl. Acad. Sci. U. S. A., 2007, 104, 9266-9271.
8. T. Maldiney, A. Bessière, J. Seguin, E. Teston, S. K. Sharma, B. Viana, A. J. J. Bos, P. Dorenbos, M. Bessodes, D. Gourier, D. Scherman and C. Richard, Nat. Mater., 2014, 13, 418-426.
9. Z. J. Li, H. W. Zhang, M. Sun, J. S. Shen and H. X. Fu, J. Mater. Chem., 2012, 22, 24713-24720.
10. L. M. Manus, D. J. Mastarone, E. A. Waters, X. Q. Zhang, E. A. Schultz-Sikma, K. W. MacRenaris, D. Ho and T. J. Meade, Nano Lett., 2009, 10, 484-489.
11. A. Louie, Chem. Rev., 2010, 110, 3146-3195.
12. J. P. Shi, H. X. Fu, X. Sun, J. S. Shen and H. W. Zhang, J. Mater. Chem. B, 2015.
13. Q. L. M. D. Chermont, C. Chaneac, J. Seguin, F. Pelle, S. Maîtrejean, J. P. Jolivet, D. Gourier, M. Bessodes and D. Scherman, PNAS, 2007, 104, 9266-9271.
14. F. Liu, W. Z. Yan, Y. J. Chuang, Z. P. Zhen, J. Xie and Z. W. Pan, Sci. Rep., 2013, 3.
15. J. Y. Park, J. H. Lee, G. S. R. Raju, B. K. Moon, J. H. Jeong, B. C. Choi and J. H. Kim, Ceram. Int., 2014, 40, 5693-5698.
16. W. B. Im, Y. Fourre, S. Brinkley, J. Sonoda, S. Nakamura, S. P. DenBaars and R. Seshadri, Opt. Express, 2009, 17, 22673-22679.
17. M. Drofenik and L. Golic, Acta Cryst., 1979, B35, 1059-1062.
18. R.D. Shannon, Acta Cryst., 1976, 32, 751-767.
19. Z. F. Tian, H. B. Liang, B. Han, Q. Su, Y. Tao, G. B. Zhang and Y. B. Fu, J. Phys. Chem. C, 2008, 112, 12524-12529.
20. L. Y. Zhou, W. C. H. Choy, J. X. Shi, M. L. Gong, H. B. Liang and T. I. Yuk, J. Solid State Chem., 2005, 178, 3004-3009.
21. X. Li, L. Guan, X. N. Li, J. W. Wen and Z. P. Yang, Powder Technol., 2010, 200, 12-15.
22. A. N. Yerpude and S. J. Dhoble, J. Lumin., 2012, 132, 2975-2978.
23. Y. H. Jin, Y. H. Hu, L. Chen, X. J. Wang and G. F. Ju, Opt. Mater., 2013, 35, 1378-1384.
24. M. D. Que, Z. P. Ci, Y. H. Wang, G. Zhu, Y. R. Shi and S. Y. Xin, J. Lumin., 2013, 144, 64-68.
25. G. Li, Y. H. Wang, S. C. Han, W. Zeng, W. B. Chen and Y. Gong, ECS J. Solid State S. C., 2013, 2, R161-R164.
26. G. Blasse, A. Bril and W. C. Nieuwpoort, Phys. Chem. Solids, 1966, 27, 1587.
27. P. C. R. S. Santos, L. C. Silva, F. A. A. Paz, R. A. S. Ferreira, J. Rocha, T. Trindade, L. D. Carlos and H. I. S. Nogueira, Cryst. Growth Des., 2008, 8, 2505-2516.
28. Sa Ferreira R. A. S., Nobre S. S., Granadeiro C. M., Nogueira H. I. S., Carlos L. D., Malta O. L., J. Lumin., 2006, 121, 561-567.
29. C. E. R. García, E.M. Tejeda, F. F. Castillon and G. A. Hirata, J. Nanosci. Nanotechno., 2011, 11, 5587-5591.
30. G. Li, Y. H. Wang, W. Zeng, S. C. Han, W. B. Chen, Y. Y. Li and H. Li, Opt. Mater., 2014, 36, 1808-1813.
31. B. Liu, C. Shi and Z. Qi, Appl. Phys. Lett., 2005, 86, 191111.
32. H. Davson, The Eye (Academic Press, 1962).
33. D. Poelman, N. Avci and P. F. Smet, Opt. Express, 2009, 17, 358-364.
34. D. Jia, W. Jia, D. R. Evans, W. M. Dennis, H. Liu, J. Zhu and W. M. Yen, J. Appl. Phys., 2000, 88, 3402-3407.
35. J. Glodo and A. Wojtowicz, J. Alloys Compd., 2000, 300, 289-294.
36. T. Kinoshita, M. Yamazaki, H. Kawazoe and H. Hosono, J. Appl. Phys., 1999, 86, 3729-3733.
37. T. Aitasalo, P. Deren, J. Hölsä, H. Junger, J. C. Krupa, M. Lastusaari, J. Legendziewicz, J. Niittykoski and W. Strek, J. Solid State Chem., 2003, 171, 114-122.
38. Y. X. Zhuang, J. Ueda and S. Tanabe, J. Mater. Chem. C, 2013, 1, 7849-7855.
39. T. Matsuzawa, Y. Aoki, N. Takeuchi and Y. Murayama, J. Electrochem. Soc., 1996, 143, 2670-2673.
40. Y. Q. Li, Y. H. Wang, Y. Gong, X. H. Xu and M. J. Zhou, Opt. Express, 2010, 18, 24853-24858.
41. D. L. Dexter, J. Chem. Phys., 1953, 21, 836.
42. J. T. Piegza and E. Zych, J. Phys. Chem. C, 2010, 114, 4215.
43. X. H. Xu, Y. H. Wang, Y. Gong, W. Zeng and Y. Q. Li, Opt. Express, 2010, 18, 16989-16994.
44. H. T. Wong, H. L. W. Chan and J. H. Hao, Appl. Phys. Lett., 2009, 95, 022512.
45. S. Y. Xin, Y. H. Wang, F. H. Li, B. T. Liu, J. Zhang and Y. Tao, J. Nanosci. Nanotechno., 2014, 14, 3743-3747.
46. S. J. Zeng, M. K. Tsang, C. F. Chan, K. L. Wong, B. Fei and J. H. Hao, Nanoscale, 2012, 4, 5118-5124.
47. N. Sarlı, Physica B, 2013, 411, 12–25.